Vehicle Dynamics Platform, Experiments, and Modeling Aiming at Critical Maneuver Handling

Kristoffer Lundahl, Jan Åslund, and Lars Nielsen

Division of Vehicular Systems, Department of Electrical Engineering
Linköping University SE-581 33 Linköping, Sweden
E-mail: kristoffer.lundahl@liu.se
Technical report: LiTH-ISY-R-3064

June 18, 2013

Abstract

For future advanced active safety systems, in road-vehicle applications, there will arise possibilities for enhanced vehicle control systems, due to refinements in, *e.g.*, situation awareness systems. To fully utilize this, more extensive knowledge is required regarding the characteristics and dynamics of vehicle models employed in these systems. Motivated by this, an evaluative study for the lateral dynamics is performed, considering vehicle models of more simple structure. For this purpose, a platform for vehicle dynamics studies has been developed. Experimental data, gathered with this testbed, is then used for model parametrization, succeeded by evaluation for an evasive maneuver. The considered model configurations are based on the single-track model, with different additional attributes, such as tire-force saturation, tire-force lag, and roll dynamics. The results indicate that even a basic model, such as the single-track with tire-force saturation, can describe the lateral dynamics surprisingly well for this critical maneuver.

CONTENTS

1 INTRODUCTION

The increasing level of sensory instrumentation and control actuators in modern vehicles, along with higher demands on traffic safety, enables and motivates more advanced safety systems for future vehicles. To exploit these opportunities in the most beneficial way, extensive knowledge in terms of vehicle handling and dynamics will be essential. Also, perhaps even more important, is insight into the vehicle characteristics certain modeling approaches are able to capture in critical situations, and the extent of their appropriateness for on-board applications.

Inspired to investigate questions raised for the above topics, a platform for vehicle-dynamics studies has been developed. This testbed, shown in Figure 1, is based on a standard car equipped with vehicle-dynamics sensor-instrumentation for highly dynamic maneuvering. Experimental data from this testbed is here used in an evaluative study, primarily considering modeling and validation of the lateral dynamics. A similar study, with more preliminary results, was presented in [1].

The intention of this study is to give a brief insight to the potential of established, simple structured, vehicle models, in terms of their ability to describe essential vehicle states and variables. With emphasis on the lateral dynamics, the considered models are based on the single-track model, extended with different additional characteristics, such as tire-force saturation, tire-force lag, and roll dynamics. To find parameters for these models, a number of experiments have been conducted, with the above mentioned vehicle testbed. Each of the model configurations was parametrized, followed by an evaluative comparison for a double lane-change maneuver.

2 EXPERIMENTAL EQUIPMENT

With the intention to offer a precise evaluation instrument for vehicle dynamics studies and applications, a vehicle testbed has been developed. The platform is based on a Volkswagen Golf V, 2008, equipped with a set of state-of-the-art sensors, measuring, *e.g.*, slip angle, roll and pitch angles, accelerations, and angular rates. In addition, information from the internal sensors are accessible over the vehicle CAN bus. This CAN access has been made possible through collaboration with Nira Dynamics AB, supporting with hardware and software interfaces to the vehicle. The additional sensors mainly consist of four different systems; an IMU, a GPS, a slip-angle sensor, and a roll/pitch measurement system. A measurement PC is used for sampling these systems, as well as for the data stream from the vehicle CAN bus. In Figure 2 a simplified scheme over the system is shown.

A more detailed description of the measurement systems and individual sensors follows below. Table 1 specifies measurement range, accuracy, and sampling frequency for the variables of most relevance.

Figure 1   The vehicle-dynamics testbed for studying critical maneuver handling.
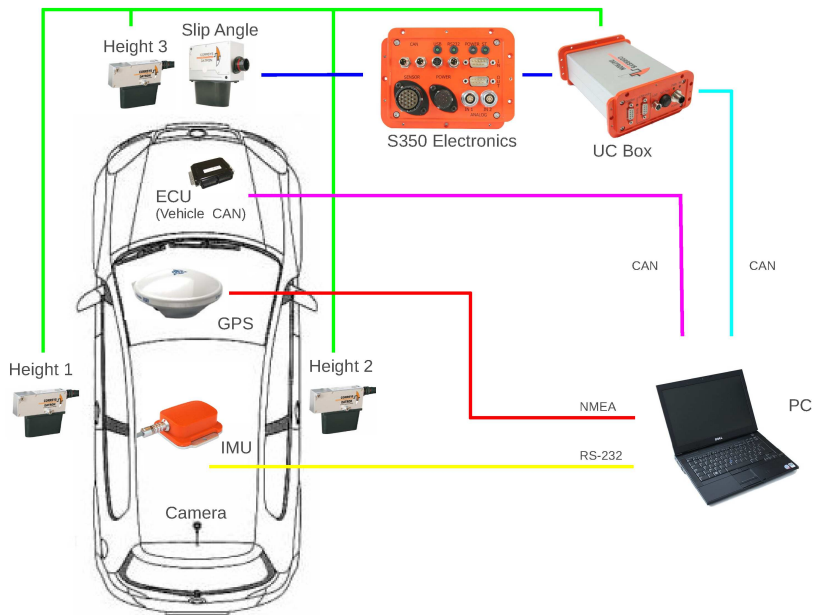
Figure 2   A schematic sketch over the measurement system.

SLIP-ANGLE SENSOR

The slip angle sensor is a Corrsys-Datron Correvit S-350. It uses optical instrumentation to measure speed and direction, with algorithms taking advantage of the irregularities in the road-surface microstructure. The sensor is mounted in the front of the vehicle, and outputs measures for the longitudinal and lateral velocities of this position. However, arbitrary points can be described, *e.g.*, the vehicle center of gravity, using these signals in combination with yaw-rate data. For further technical specifications see [2].

ROLL AND PITCH ANGLE MEASUREMENT SYSTEM

The system for roll and pitch angle measurement mainly consists of three height sensors, Corrsys-Datron HF-500C, mounted around the vehicle, and thereby mapping the plane of the vehicle body relative the ground. The sensors emit a visible laser at the road surface, and determine the height from the reflected light beam. The accuracies of the measured roll and pitch angles are linearly correlated to the relative placement of the sensors, assuming chassis deflections are neglected. For further technical specifications see [3].

IMU — ACCELEROMETER AND GYROSCOPE

The *inertial measurement unit*, IMU, is an Xsens MTi, measuring accelerations and angular rates in three dimensions. Additionally, it has a built in magnetometer for possible yaw angle measurements, however, the responsiveness of this is a bit too slow for rapid vehicle dynamics studies. For further technical specifications see [4].

GPS

For vehicle positioning a GPS module of u-blox AEK-4P type is used. For more specific information see [5].

INTERNAL SENSORS

On the vehicle CAN bus several sensors, with relevance for vehicle dynamics applications, are accessible at a sampling rate of 10 Hz. Many of these are redundant due to the additional sensors, and of worse

quality in terms of accuracy and noise. However, signals for steering wheel angle and wheel angular velocities are of great importance since no additional equipment has been added to sample these, or equivalent variables.

TEST TRACK

Through a collaborative effort with Linköpings Motorsällskap, LMS, permission has been given to access their race and test track, Linköpings Motorstadion. Figure 3 illustrates a double lane-change maneuver at this facility.

Table 1   Technical specifications for the additional sensors.

Variable	Range	Accuracy	Frequency
Corrsys-Datron Correvit S-350			
Long. velocity, v_x	0.5–250 km/h	0.1 %	250 Hz
Lateral velocity, v_y		0.1 %	250 Hz
Slip angle, β	± 40 deg	0.1 deg	250 Hz
Corrsys-Datron HF-500C			
Height	125–625 mm	0.2 %	250 Hz
Roll angle, ϕ	± 15 deg	0.08 deg	250 Hz
Pitch angle, θ	± 11 deg	0.06 deg	250 Hz
Xsens MTi			
Accelerations a_x, a_y, a_z	± 17 m/s^2	0.02 m/s^2	100 Hz
Angular rates $\dot{\phi}, \dot{\theta}, \dot{\psi}$	± 300 deg/s	0.3 deg/s	100 Hz
u-blox AEK-4P			
Position (GPS)		2.5 m	4 Hz

Figure 3   A double lane-change maneuver at Linköpings Motorstadion.

3 VEHICLE MODELING

The vehicle models that will be evaluated are of a simple structure, *e.g.*, neglecting load transfer and individual wheel-dynamics. The model configurations use the single-track model as a basis, to describe the lateral dynamics of the vehicle, coupled to tire models of different complexity. Additionally, an extended version of the single-track model is considered, where roll dynamics has been added. The number of considered model configurations adds up to a total of four.

SINGLE-TRACK MODEL

The single-track model is a simplified planar model describing the chassis dynamics, with left and right wheels lumped into a single front and a single rear wheel, see, *e.g.*, [6]. The model is illustrated in Figure 4, and has its dynamics described by

$$m(\dot{v}_y + v_x\dot{\psi}) = F_{y,f}\cos(\delta) + F_{y,r} + F_{x,f}\sin(\delta), \tag{1}$$

$$I_{zz}\ddot{\psi} = l_f F_{y,f}\cos(\delta) - l_r F_{y,r} + l_f F_{x,f}\sin(\delta), \tag{2}$$

where m represents the total vehicle mass, I_{zz} the yaw inertia, l_f, l_r the distances from front and rear wheel axles to the center of gravity (CoG), δ the steer angle for the front wheels, v_x, v_y the longitudinal and lateral velocity at the CoG, $\dot{\psi}$ the yaw rate, and F_x, F_y longitudinal and lateral tire forces for the front and rear wheels. Since this study is focused on the lateral dynamics, no longitudinal excitations will be considered, hence, $F_{x,f} = 0$.

SINGLE TRACK WITH ROLL DYNAMICS

An extended variant of the above single-track model is also considered, where the roll angle, ϕ, has been added as an additional degree of freedom, *i.e.*, the rotational motion about the *x*-axis, as depicted in Figure 5. Thus, the motion dynamics follows from

$$m(\dot{v}_y + v_x\dot{\psi}) - m_s h\ddot{\phi} = F_{y,f}\cos(\delta) + F_{y,r} + F_{x,f}\sin(\delta), \tag{3}$$

$$I_{zz}\ddot{\psi} = l_f F_{y,f}\cos(\delta) - l_r F_{y,r} + l_f F_{x,f}\sin(\delta), \tag{4}$$

$$I_{xx}\ddot{\phi} + D_\phi\dot{\phi} + K_\phi\phi = m_s h a_y. \tag{5}$$

Here m_s is the sprung mass of the vehicle body, I_{xx} the roll inertia, h the distance between CoG and the roll center, K_ϕ the roll stiffness, and D_ϕ the roll damping. The lateral acceleration a_y is described by the following relation,

$$a_y = \dot{v}_y + v_x\dot{\psi}.$$

Note that the variables v_x, v_y, and a_y, in this model, describe the motions of the roll center, rather than the CoG (which is moving from side to side, relative the remaining chassis dynamics).
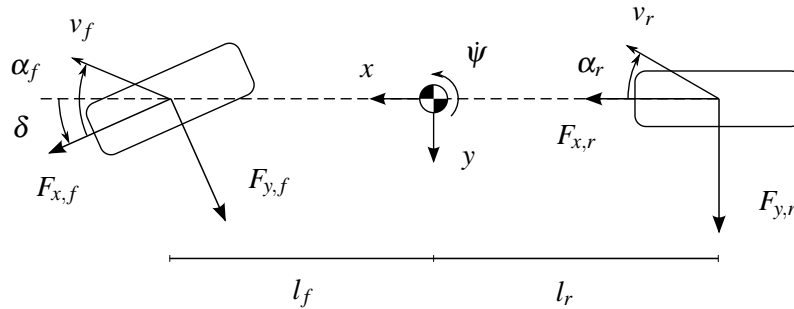

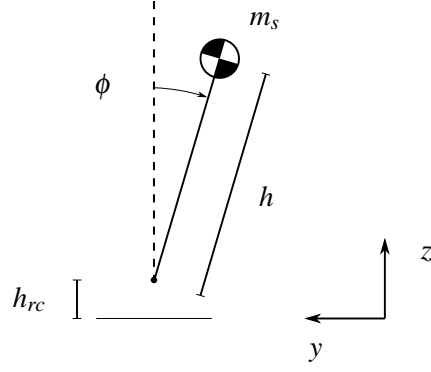*Figure 4   The single-track model.*

Figure 5   Illustration of the roll dynamics.

3.1 TIRE MODELING

For the tire modeling, three different models of various complexity are considered; a linear model, a nonlinear model, and a nonlinear model capturing tire-force lag. The slip angle, α, is defined as

$$\alpha_f = \delta - \arctan\left(\frac{v_y + l_f\dot{\psi}}{v_x}\right), \tag{6}$$

$$\alpha_r = -\arctan\left(\frac{v_y - l_r\dot{\psi}}{v_x}\right), \tag{7}$$

for the front and rear axles, following the definitions in [7].

LINEAR TIRE-MODEL

The *linear tire-model* assumes a linear relation between the tire force and slip angle, described by

$$F_{y,i} = C_{\alpha,i}\alpha_i, \quad i = f, r, \tag{8}$$

where $C_{\alpha,f}, C_{\alpha,r}$ are the cornering stiffness for the front and rear axles.

MAGIC FORMULA

To represent the nonlinear force–slip tire characteristics, the *Magic Formula* tire model, [7], has been considered. The model is described by

$$F_{y,i} = \mu_{y,i}F_{z,i}\sin(C_{y,i}\arctan(B_{y,i}\alpha_i - E_{y,i}(B_{y,i}\alpha_i - \arctan B_{y,i}\alpha_i))), \tag{9}$$

with $i = f, r$. Here μ_y represent the lateral friction-coefficient and $C_{y,i}$, $E_{y,i}$ are model parameters, while $B_{y,i}$ can be calculated from

$$B_{y,i} = \frac{C_{\alpha,i}}{C_{y,i}\mu_{y,i}F_{z,i}}.$$

The normal loads, $F_{z,f}$ and $F_{z,r}$, are here considered static, since no load transfer is included in the chassis model. Hence, they are given by

$$F_{z,f} = mg\frac{l_r}{l}, \quad F_{z,r} = mg\frac{l_f}{l}, \tag{10}$$

where g is the gravity constant and l the wheel base according to $l = l_f + l_r$.

RELAXATION LENGTH

Due to compliences in the tire structure, a reduced response appears for the lateral tire-forces. This force lag can be described by a *relaxation length*, σ, introducing a time-delay for the slip angles, [7]. The delayed slip angle, denoted α^*, is described by

$$\dot{\alpha}_i^*\frac{\sigma}{v_{x,i}} + \alpha_i^* = \alpha_i, \quad i = f, r. \tag{11}$$

7

This slip angle is then used in the tire-force equation, thereby forming a delayed tire-force response. The relaxation-length model will here only be used together with the Magic Formula tire-model, where F_y is described, analogous to (9), as

$$F_{y,i} = \mu_{y,i} F_{z,i} \sin(C_{y,i} \arctan(B_{y,i} \alpha_i^* - E_{y,i}(B_{y,i} \alpha_i^* - \arctan B_{y,i} \alpha_i^*))), \tag{12}$$

with $i = f, r$.

3.2 MODEL CONFIGURATIONS

The four different model configurations, composed of the above submodels, are the following:

- Single-track model, (1)–(2), with the linear tire model, (8).

- Single-track model, (1)–(2), with the Magic Formula tire model, (9).

- Single-track model, (1)–(2), with the Magic Formula tire model and relaxation length, (11)–(12).

- Single-track model with roll dynamics, (3)–(5), and the Magic Formula tire model, (9).

These models are summarized in Table 2, where also the corresponding model notations are stated.

Table 2 Notations for the considered model configurations.

Model	Notation
Single-track with linear tire-model	ST-L
Single-track with Magic Formula	ST-MF
Single-track with Magic Formula and relaxation length	ST-MF-RL
Single-track with roll dynamics and Magic Formula	ST-Roll-MF

4 TEST SCENARIOS

Three different test scenarios, for parametrization and validation purposes, have been considered. The tests were held at Linköpings Motorstadion, using the vehicle testbed presented in Section 2.

The *slalom test* consists of seven lined up cones, separated by 17 m. The vehicle is driven through the course, in a slalom pattern, at constant speed.

The *double lane-change maneuver* is a standardized test, often used for vehicle stability evaluations, [8]. An overview sketch is shown in Figure 6.

An additional test, here referred to as the *rock'n'roll test*, is carried out for the vehicle at stand-still. The sprung body is pushed from the side, or *rocked* back and forth, initiating in a vibrating motion in the *roll* direction. Hence the name; the vehicle is *rocked* and then *rolls*. The sequence of interest is when the vehicle body is left to roll-vibrate freely, with no external forces being applied.

The experiments above have been conducted at two separate occasions, under slightly different weather conditions. The vehicle parameters, such as inertia and mass properties, are considered equal for
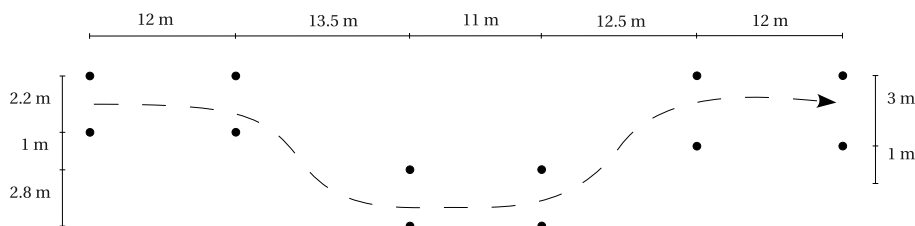

Figure 6 A sketch over the double lane-change maneuver.

both occasions, however, the tire parameters are not. Therefore, when referring to the measurement data, two separate batches are considered; *measurement batch 1* and *measurement batch 2*. The first batch consists of 26 different double lane-change maneuvers with different entry speeds. The second batch includes seven slalom runs, two double lane-change maneuvers, and the rock'n'roll test for two different load cases (normal load-condition and with a 75 kg roof load).

5 MODEL PARAMETER ESTIMATION

The parametrization, for the models in Section 3, has been carried out with established estimation methods, on data sets gathered with the vehicle testbed presented in Section 2.

5.1 ESTIMATION METHOD

A *prediction-error identification method* (PEM), [9], has been used for the parameter estimations. Consider a system represented by

$$\dot{x}(t, \theta) = f(x(t), u(t); \theta), \tag{13}$$

$$y(t, \theta) = h(x(t, \theta), u(t); \theta) + e(t), \tag{14}$$

with x being the state vector, u the input, y the system output (*i.e.*, the measurements), e the measurement noise and θ the parameter set. A prediction for the output of this system, $\hat{y}$, can then be formulated according to

$$\dot{\hat{x}}(t, \theta) = f(\hat{x}(t, \theta), u(t); \theta), \tag{15}$$

$$\hat{y}(t, \theta) = h(\hat{x}(t, \theta), u(t); \theta), \tag{16}$$

where $\hat{x}$ represent the estimated state vector. A cost function, V, based on the predictive error, ε, is then defined as

$$\varepsilon(t, \theta) = y(t, \theta) - \hat{y}(t, \theta), \tag{17}$$

$$V(\theta) = \frac{1}{N} \sum_{t_0}^{t_N} \varepsilon(t, \theta)^T W \varepsilon(t, \theta), \tag{18}$$

for the measurement set of N samples. The weighting matrix W is a diagonal matrix which enables the user to weight the different error predictions against each other, based on noise, relative magnitude, or confidence to a specific sensor. The estimated parameter set, $\hat{\theta}$, is then found by minimizing the cost function,

$$\hat{\theta} = \arg \min_{\theta} V(\theta). \tag{19}$$

To perform this estimation procedure, the MATLAB toolbox *System Identification Toolbox*, [10], has been utilized.

5.2 VEHICLE PARAMETERS

The vehicle parameters that need to be determined, are the ones used in (1)–(2) and (3)–(5), being m, l_f, l_r, and I_{zz}, if temporarily neglecting parameters for the roll dyanmics (they will be treated below). The total vehicle mass, m, and CoG-to-wheel-axis distances, l_f and l_r, have been determined in a more straightforward fashion, not utilizing the above estimation routine, with a vehicle scale and manual tape-measuring. To determine the yaw inertia, I_{zz}, data from five different slalom runs and two double lane-change runs were used, belonging to measurement batch 2. The estimation method was then employed to determine I_{zz} and the complete set of tire parameters for the ST-MF model (using ST-MF-RL or ST-Roll-MF instead, results in equivalent values for I_{zz}). Since, the validation procedure will consider measurement batch 1, and the tire parameters found here only are valid for measurement batch 2, these are discarded.

ROLL DYNAMICS PARAMETERS

To determine the parameters corresponding to the roll dynamics, data from the stand-still rock'n'roll test was used. In (5), five parameters appear; I_{xx}, D_ϕ, K_ϕ, m_s, and h, but only three lumped parameters can be distinguished from this equation;

$$\frac{D_\phi}{I_{xx}}, \quad \frac{K_\phi}{I_{xx}}, \quad \text{and} \quad \frac{m_s h}{I_{xx}}.$$

However, in (3) $m_s h$ appears apart from I_{xx}. Thus, as a minimum, the following four parameters need to be determined;

$$I_{xx}, \quad D_\phi, \quad K_\phi, \quad \text{and} \quad m_s h.$$

For this purpose, two different load cases of the rock'n'roll test was used; no additional loading and a 75 kg roof-load. The roof load was here treated as a point mass, $m_{aux} = 75$ kg, located $h_{aux} = 1.60$ m above ground, thus, contributing with an additional roll inertia of $I_{aux} = m_{aux}(h_{aux} - h_{rc})^2$.

If the vehicle is considered to vibrate freely about the roll axis, which is the case for the rock'n'roll tests, this implies no external forces are present, *i.e.* $a_y = 0$. Thus, (5) can therefore be rewritten as

$$I_{xx}\ddot{\phi} + D_\phi\dot{\phi} + K_\phi\phi = 0,$$

for the normal load-case and

$$(I_{xx} + I_{aux})\ddot{\phi} + D_\phi\dot{\phi} + K_\phi\phi = 0,$$

for the load case with a roof load. Applying the estimation method on these two equations, with data from the rock'n'roll tests, the lumped parameters in Table 3 can be determined. These four parameters forms an overdetermined system for the unknown parameters, I_{xx}, D_ϕ, and K_ϕ, which is solved with the least square method.

The remaining roll parameters, *i.e.*, the lumped parameter $m_s h$ and the roll-center height h_{rc}, was subsequently estimated simultaneously with the tire parameters, from the double lane-change tests. Here the relation

$$a_y = a_{y,imu} + (h_{imu} - h_{rc})\ddot{\phi},$$

was utilized to determine h_{rc}, where a_y represent the lateral acceleration at the roll center, while $a_{y,imu}$ is the lateral acceleration the IMU sensor sees, *i.e.*, at a distance $h_{imu} = 0.40$ m from the ground.

In Table 4 all the determined vehicle parameters are specified, with corresponding standard deviations for I_{zz}, $m_s h$, and h_{rc}. The low magnitude of these standard deviations, in relation to the parameter values, indicates a confident estimate for these parameters. Standard deviations are not specified for m, l_f, and l_r since no estimation method has been involved to acquire them, and neither for I_{xx}, D_ϕ, and K_ϕ because they are simply least-square values from the parameters in Table 3. For all the parameters in Table 4, reasonable values are obtained when considering physical dimensions. Except for the lumped parameter $m_s h$. The sprung mass m_s is only a subset of the total mass m, thus, $m_s < m$. However, for this condition to hold, the CoG-to-roll-center height needs to be $h > 0.57$ m. This implies a CoG height of $h > 0.74$ m, which by physical means, seems a bit high. This indicates that the lumped parameter $m_s h$ is capturing characteristics beside the physical quantities m_s and h, or that it compensates for poor parametrization of, *e.g.*, the roll inertia or roll stiffness/damping.

Table 3   Estimated lumped roll-dynamics parameters.

Load case	Notation	Value	Std. dev.
No load	D_ϕ/I_{xx}	7.255	0.045
	K_ϕ/I_{xx}	173.2	0.57
Roof load	$D_\phi/(I_{xx}+I_{aux})$	5.617	0.029
	$K_\phi/(I_{xx}+I_{aux})$	138.5	0.32

Table 4   Vehicle parameters.

Notation	Value	Unit	Std. dev.
m	1415	kg	-
l_f	1.03	m	-
l_r	1.55	m	-
I_{zz}	2581	kgm^2	13.5
I_{xx}	616	kgm^2	-
D_ϕ	4390	Nms/rad	-
K_ϕ	106600	Nm/rad	-
$m_s h$	807	kgm	0.67
h_{rc}	0.165	m	0.0046

5.3 TIRE PARAMETERS

The tire parameters were determined from 23 different double lane-change runs, sampled in measurement batch 1, leaving three tests from this batch for validation purpose (see the following section). The tire parameters were estimated for ST-MF, ST-MF-RL, and ST-Roll-MF separately, and is summarized in Table 5 with corresponding standard deviations. For ST-L, the cornering stiffness, $C_{\alpha,f}$ and $C_{\alpha,r}$—being the only tire parameters for this model—were taken from the estimated ST-MF parameter-set. In Figure 7 the force–slip characteristics is shown for the different estimated parameter-sets. Here the cornering stiffness seems less stiff for ST-MF, compared to ST-MF-RL and ST-Roll-MF, which is congruent with the specified values for C_α in Table 5. Since ST-MF does not incorporate any kind of response delay, such as relaxation length in ST-MF-RL or the roll dynamics in ST-Roll-MF, it compensates for this with a more compliant force model. Also, the cornering stiffness for the front wheels is lower, compared the rear-wheel cornering-stiffness, for all models. This should be a combined effect of different normal loads, F_z, on the wheel axes, as well as more compliance in front suspension and steering. For the rear wheel force–slip curves in Figure 7, considerable deviations between the models can be seen for slip angles $\alpha > 0.07$ rad. This is a result of a limited number of data samples in this region, which is also indicated by the high standard deviations for C_y and E_y, suggesting these are unreliable parameter values. The characteristics seen in this region is therefore purely an extrapolated effect of the parametrization at lower slip angles. However, this will only be an issue if the vehicle models are subjected to maneuvers provoking very large slip angles.

Table 5   Estimated tire parameters.

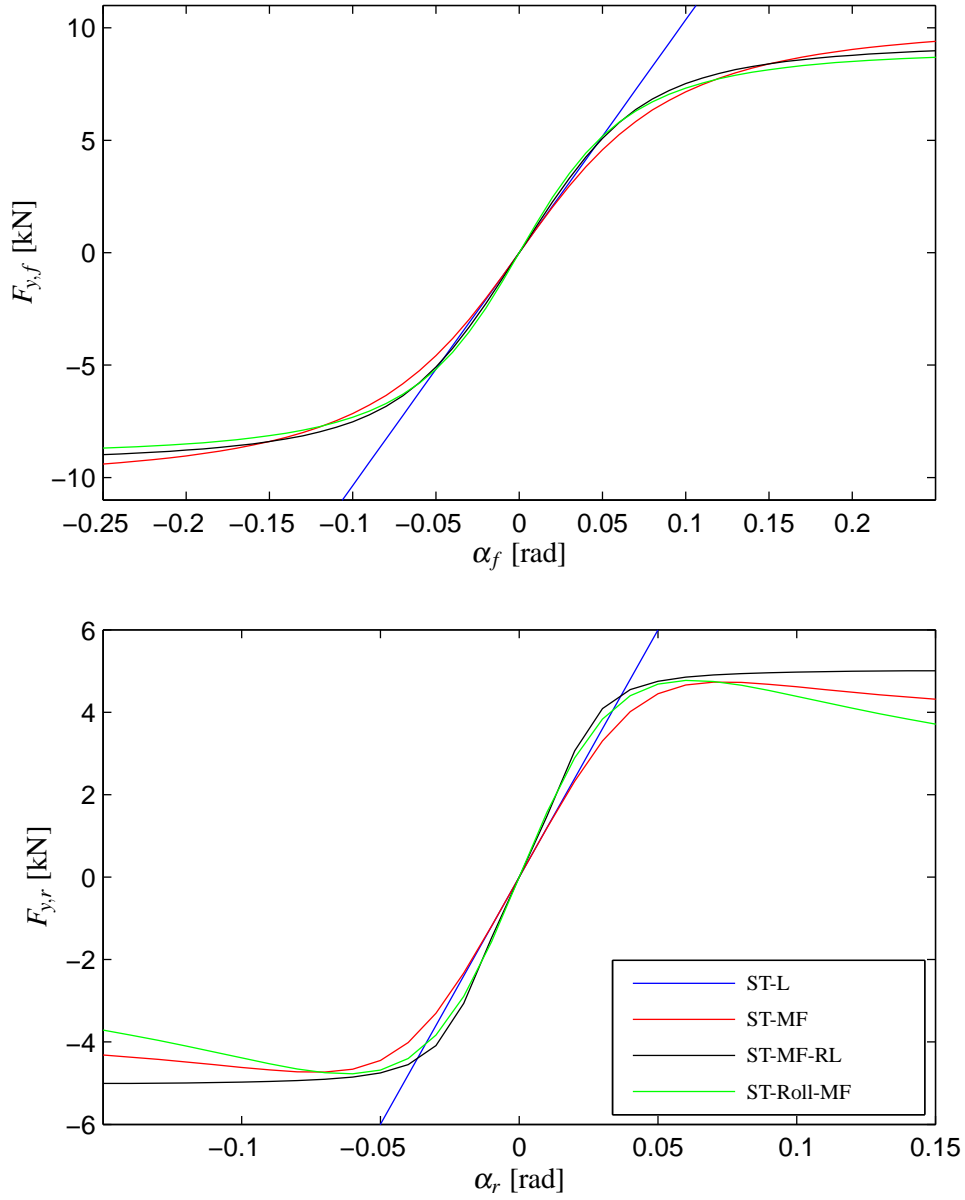| Notation	ST-MF Value	ST-MF Std. dev.	ST-MF-RL Value	ST-MF-RL Std. dev.	ST-Roll-MF Value	ST-Roll-MF Std. dev.
$C_{\alpha,f}$	103600	701	114600	648	128200	881
$C_{\alpha,r}$	120000	1288	138400	1923	162300	991
$\mu_{y,f}$	1.20	0.079	1.12	0.019	1.07	0.062
$\mu_{y,r}$	0.85	0.002	0.91	0.011	0.86	0.001
$C_{y,f}$	1.15	0.86	0.809	0.026	1.13	0.78
$C_{y,r}$	1.46	0.055	0.924	0.031	1.82	0.13
$E_{y,f}$	0.41	2.18	-0.73	0.073	0.354	1.51
$E_{y,r}$	-1.55	0.19	-4.47	0.28	-0.029	0.22
σ	-	-	0.571	0.0066	-	-

Figure 7   Tire forces vs slip angles, for the different models.

6 MODEL VALIDATION AND ANALYSIS

As a basis for the model validation, data from three double lane-change tests, belonging to measurement batch 1, were used. These tests were employed with different initial speeds, thus, triggering various levels of dynamics. The tests are denoted Test 1, Test 2, and Test 3, corresponding to the results shown in Figure 8, 9 and 10. In these figures, measurement data for yaw rate $\dot{\psi}$, lateral acceleration a_y, front slip-angle α_f, and rear slip-angle α_r are displayed along with simulated data for the models in Section 3, with the parameter sets from Section 5. In Figure 11–13 the measured roll angle is compared to the simulated for ST-Roll-MF. The simulation results are acquired with an ODE solver, using steer-wheel angle δ and longitudinal velocity v_x from the measurement data as input signals. Table 6 specifies the initial velocity v_{init} and maximum values for steering-wheel angle δ_{sw}, steering-wheel-angle rate-of-change $\dot{\delta}_{sw}$, yaw rate $\dot{\psi}$, lateral acceleration a_y, slip angle α, and slip-angle rate-of-change $\dot{\alpha}$, corresponding to measurement data for Test 1–3. Notice that δ_{sw} here denotes the angle the driver is turning the steering wheel, unlike δ, which denotes the steer angle of the front wheels. The values in Table 6 give a representative overview for the tests, indicating the nature of each test run. The fundamental differences between these runs are the different entry speeds, which propagates to affect the overall behavior. A higher entry speed requires more rapid maneuvering, in terms of $\dot{\delta}_{sw}$, resulting in higher values for $\dot{\psi}$, a_y, α, and $\dot{\alpha}$.

In Figure 8, showing results for Test 1, the different models produce very consistent behavior, with good agreement to the experimental data. This is natural since the maneuvering mainly is making use of the linear region of the tire models, which is indicated by the measured maximum slip-angle values, $\alpha_{f,max}$ and $\alpha_{r,max}$, in Table 6. Although this test would be considered as quite a hefty maneuver compared to normal driving, for example in terms of $a_{y,max}$ and $\dot{\delta}_{sw,max}$, it is still not enough to trigger notable effects from relaxation length or roll dynamics.

For Test 2, in Figure 9, larger tire forces are required to handle the more rapid dynamics. Hence, slip angles outside of the linear region are utilized, see Figure 7. The ST-L model therefore becomes less valid for these parts of the maneuver, being most obvious for $\dot{\psi}$ and a_y around $t = 2.7$ s. For the other three models, only minor differences appear.

In Test 3, more distinct differences appear for the different models, see Figure 10. This is simply a consequence of the faster and more aggressive level of dynamics, *e.g.*, in terms of $a_{y,max}$, $\dot{\alpha}_{f,max}$, and $\dot{\alpha}_{r,max}$, that comes with the higher entry speed. The differences are most pronounced towards the end of the maneuver, while for the first half they all show remarkably similar behavior, following the measurement well. For the second half, ST-L is off by quite a margin. Both ST-MF and ST-MF-RL follow the measurement data by similar means, although, ST-MF-RL seems to be able to capture the most rapid characteristics slightly more accurate. ST-Roll-MF, on the other hand, shows quite erroneous behavior for the last half second of the maneuver, where the rear slip-angle encounters a large overshoot at $t = 3.5$ s, subsequently affecting other variables. This overshoot-tendency can also be seen at $t = 2.8$ s.

Table 6   Initial velocity and maximum values, for a few selected variables, corresponding to the measurement data for Test 1–3. Note that δ_{sw} refers to the steering wheel angle.

Variable	Test 1	Test 2	Test 3	Unit
v_{init}	38.3	51.4	62.4	km/h
$\delta_{sw,max}$	154	147	157	deg
$\dot{\delta}_{sw,max}$	615	742	1013	deg/s
$\dot{\psi}_{max}$	0.535	0.586	0.710	rad/s
$a_{y,max}$	5.78	7.96	9.23	m/s^2
$\alpha_{f,max}$	0.062	0.097	0.124	rad
$\alpha_{r,max}$	0.034	0.060	0.102	rad
$\dot{\alpha}_{f,max}$	0.386	0.551	0.814	rad/s
$\dot{\alpha}_{r,max}$	0.239	0.400	0.690	rad/s

The reason for this behavior, is mainly due to the tire-model parametrization. In Figure 7, $F_{y,r}$ for ST-Roll-MF decays fast for $\alpha_r > 0.07$ rad, compared to the other models. Thus, for rear slip-angles of this magnitude, ST-Roll-MF is unable to produce large enough $F_{y,r}$, resulting in an increasing α_r.

Considering the roll angle behavior in Test 1 and 2, as well as the first part of Test 3, see Figure 11–13, ST-Roll-MF captures the overall roll-angle dynamics very well. Except around some of the peak values, which might be an indication of erroneous roll-parameters or nonlinear characteristics in the roll dynamics, that could contribute to false simulation behavior or tire-model parametrization (such as the fast decay of $F_{y,r}$, discussed above).

7   CONCLUSIONS

A vehicle dynamics testbed has been developed, for the purpose of studying road-vehicle behavior and characteristics in aggressive and rapid maneuvers. A parametrization procedure is subsequently presented, determining individual vehicle and tire parameters for different model configurations, from measurement data gathered with the vehicle testbed. The treated models capture various dynamic properties, such as tire-force saturation, tire-force lag, and roll dynamics. Data for a double lane-change maneuver has then been used for validating and analyzing the dynamic characteristics of these models with their corresponding parameter sets.

The study shows that for an evasive maneuver, a simple model—such as the single-track with a tire model capturing the tire-force saturation—can predict the lateral dynamics well, even for very quick and rapid maneuvering. Additional complexity could be added, *e.g.*, by introducing tire-force lag, but the gain in accuracy is minor. This is promising for further studies on the subject, indicating that less complex vehicle-models might be accurate enough for certain critical-maneuvering applications. However, for more convincing conclusions to be established, additional thorough investigations will be needed, *e.g.*, considering combined lateral and longitudinal dynamics.
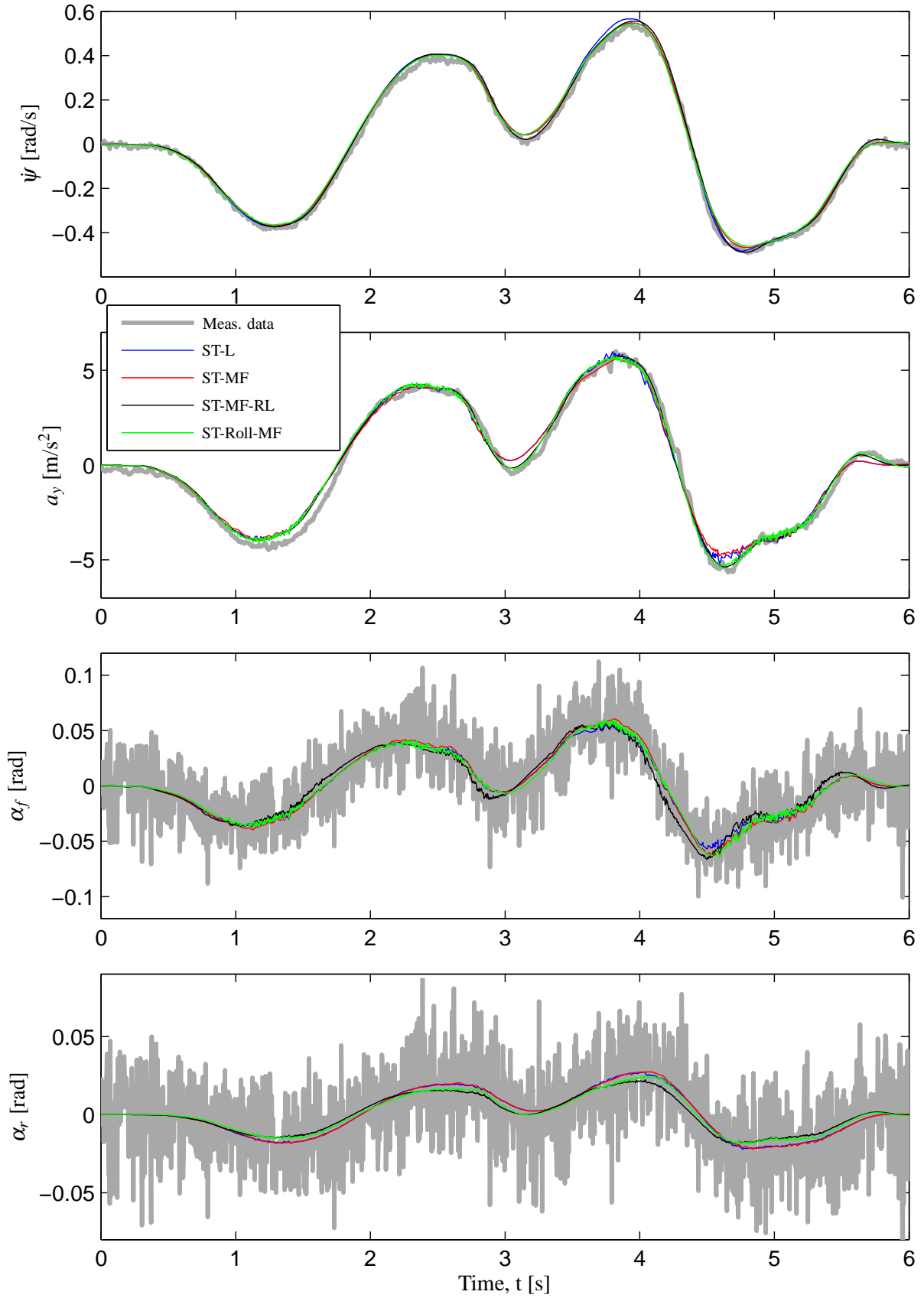
Figure 8   Measurement data compared to simulations of ST-L, ST-MF, ST-MF-RL, and ST-Roll-MF for Test 1, i.e. *a double lane-change maneuver with initial velocity of* $v_{init} = 38$ *km/h.*
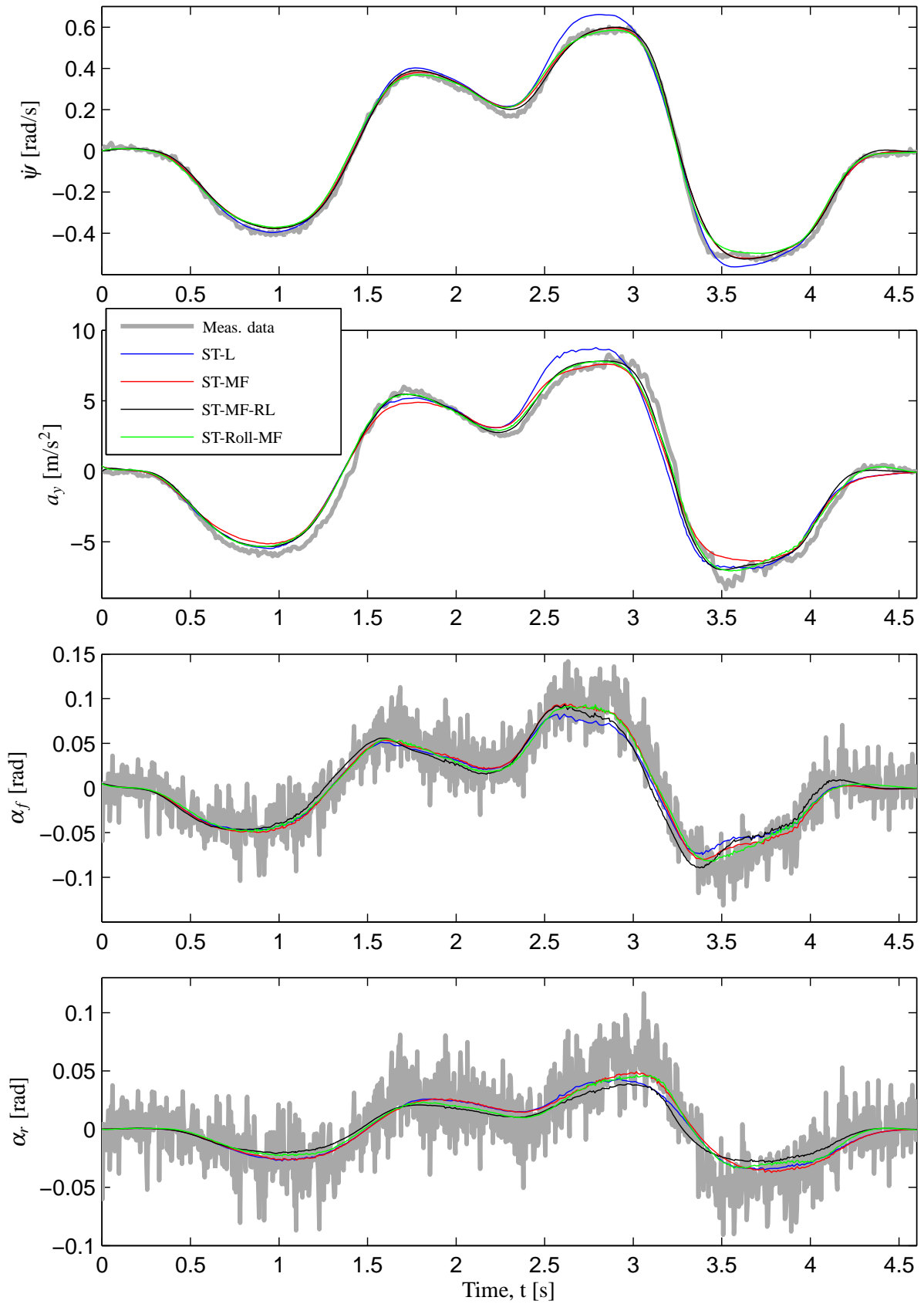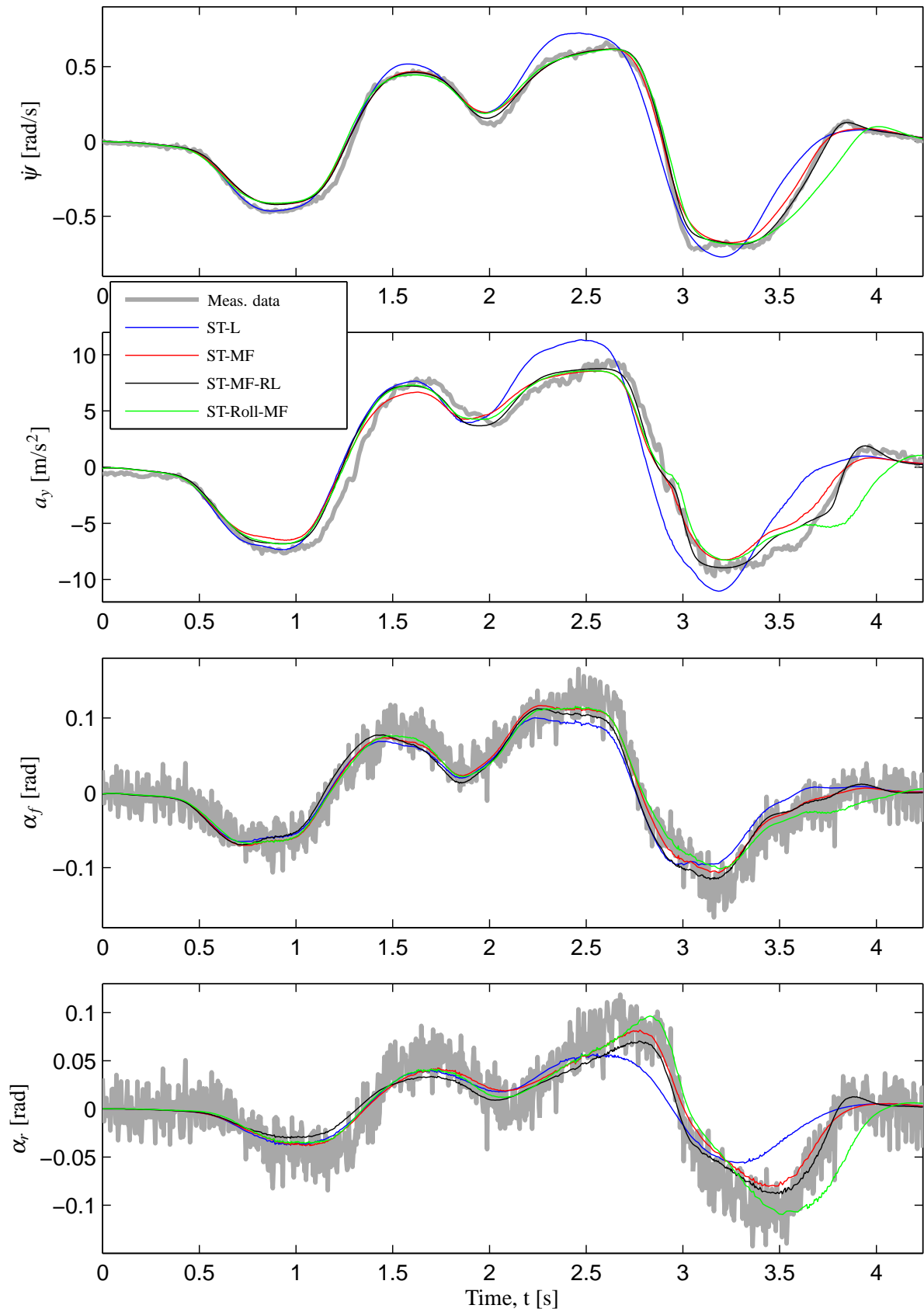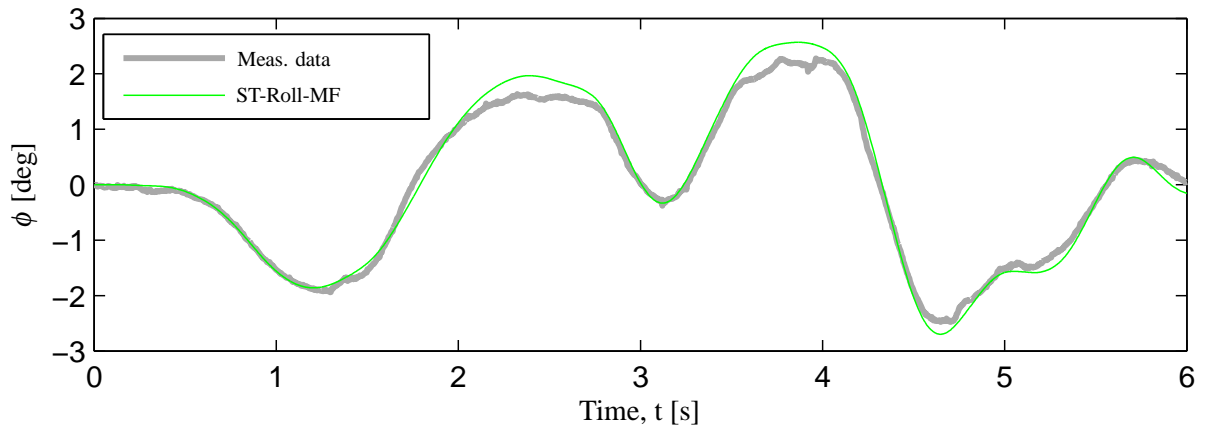
Figure 9   Measurement data compared to simulations of ST-L, ST-MF, ST-MF-RL, and ST-Roll-MF for Test 2, i.e. *a double lane-change maneuver with initial velocity of* $v_{init} = 51$ *km/h.*

Figure 10   Measurement data compared to simulations of ST-L, ST-MF, ST-MF-RL, and ST-Roll-MF for Test 3, i.e. *a double lane-change maneuver with initial velocity of v_init = 62 km/h.*

Figure 11   Roll-angle measurement compared to simulation with ST-Roll-MF, for Test 1.
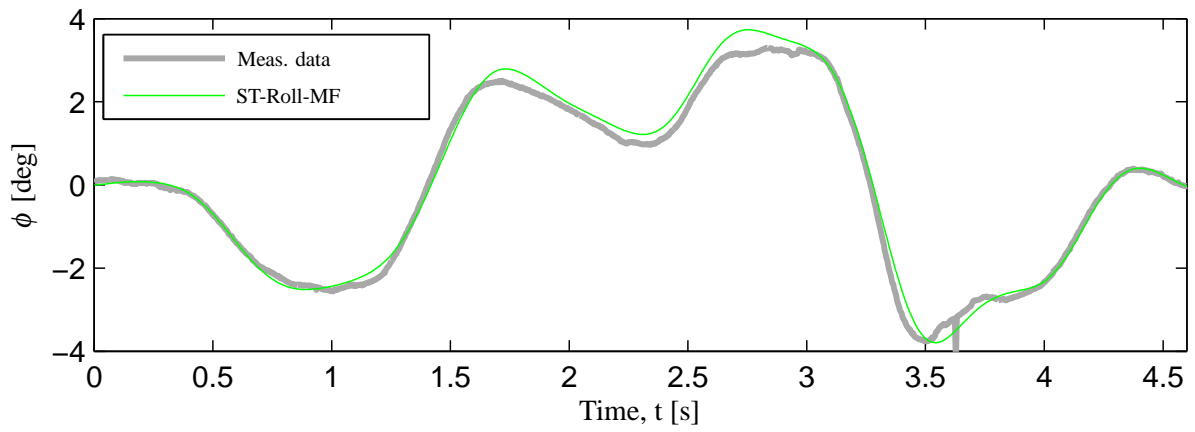

Figure 12   Roll-angle measurement compared to simulation with ST-Roll-MF, for Test 2.
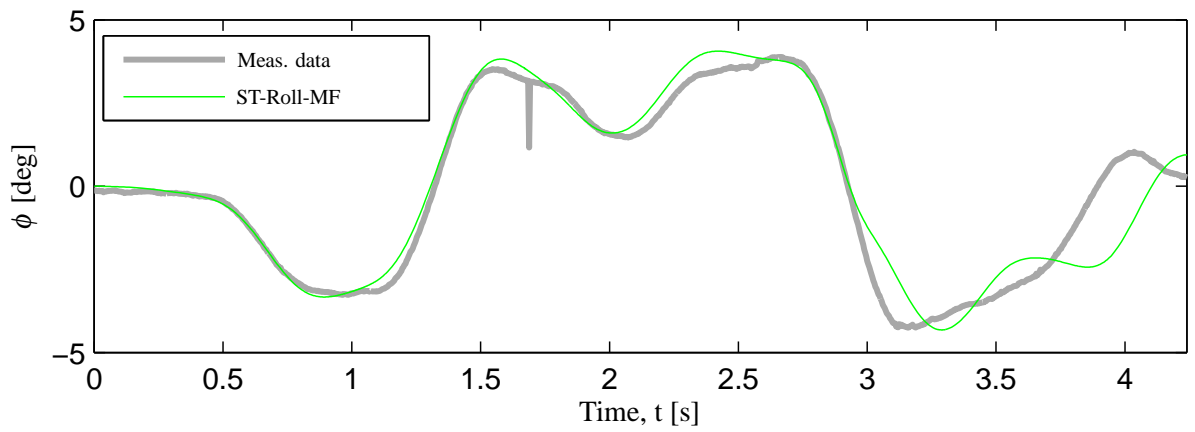

Figure 13   Roll-angle measurement compared to simulation with ST-Roll-MF, for Test 3.

REFERENCES

[1] K. Lundahl, J. Åslund, and L. Nielsen, "Investigating vehicle model detail for close to limit maneuvers aiming at optimal control," in *22nd Int. Symp. on Dynamics of Vehicles on Roads and Tracks (IAVSD)*, (Manchester, United Kingdom), 2011.

[2] Corrsys-Datron Sensorsysteme GmbH, *CORREVIT S-350 Aqua, Non-contact 2-axis Optical Sensor for Slip Free Measurement of Longitudinal and Transversal Dynamics, User Manual Volume I*, 2009.

[3] Corrsys-Datron Sensorsysteme GmbH, *HF Sensors, HF-250C/HF-500C/HF-750C, Optical Laser Height Sensor with CORREVIT SF Housing Profile for Non-contact Distance Measurement, User Manual Volume I*, 2009.

[4] Xsens Technologies B.V., *MTi and MTx User Manual and Technical Documentation*, 2009.

[5] u-blox AG, *AEK-4P, AEK-4H, GPS and SuperSense Evaluation Kits, ANTARIS 4 Positioning Engine*, 2005.

[6] J. Wong, *Theory of Ground Vehicles*. John Wiley & Sons, INC, Ottawa, Canada, fourth ed., 2008.

[7] H. B. Pacejka, *Tire and Vehicle Dynamics*. Oxford, United Kingdom: Butterworth-Heinemann, second ed., 2006.

[8] ISO 3888-2:2011, *Passenger cars — Test track for a severe lane-change manoeuvre — Part 2: Obstacle avoidance*. Geneva, Switzerland: International Organization for Standardization, 2011.

[9] L. Ljung, *System Identification: Theory for the User, 2/e*. Prentice Hall, second ed., 1999.

[10] The MathWorks, Inc., "MATLAB: System Identification Toolbox," 2013.